

Article

A New Five-Port Energy Router Structure and Common Bus Voltage Stabilization Control Strategy

Xianyang Cui ^{1,2}, Yulong Liu ^{1,2} , Ding Yuan ^{1,2}, Tao Jin ^{1,2,*} and Mohamed A. Mohamed ^{3,*} ¹ College of Electrical Engineering and Automation, Fuzhou University, Fuzhou 350108, China² Fujian Province University Engineering Research Center of Smart Distribution Grid Equipment, Fuzhou 350108, China³ Electrical Engineering Department, Faculty of Engineering, Minia University, Minia 61519, Egypt

* Correspondence: jintly@fzu.edu.cn (T.J.); dr.mohamed.abdelaziz@mu.edu.eg (M.A.M.)

Abstract: Multi-port energy routers are a core device that integrates distributed energy sources and enables energy-to-energy interconnections. For the energy routing system, the construction of its topology, the establishment of internal model switching and the control of common bus voltage stability are the key elements of the research. In this paper, a five-port energy router structure is proposed, including a PV port, an energy storage port, a grid-connected port, a DC load port, and an AC load port. Among them, the energy storage port and the grid-connected port involve bidirectional energy flow, which are the core ports of control. For the system state, a model switching strategy is proposed based on the topology and the port energy flow direction. When the external conditions change, the system can be stabilized by means of a quick response from the energy storage port. When the energy storage is saturated, the state is switched, and the grid-connected port works to achieve system stability. The rapid stabilization of the bus voltage and the free flow of energy are achieved by combining the fast response of the model predictive control with the properties of multiple model switching. Finally, the feasibility of this energy router topology and control strategy is verified by building simulations in MATLAB.

Keywords: energy internet; energy router; common bus voltage; cooperative control; model transformation



Citation: Cui, X.; Liu, Y.; Yuan, D.; Jin, T.; Mohamed, M.A. A New Five-Port Energy Router Structure and Common Bus Voltage Stabilization Control Strategy. *Sustainability* **2023**, *15*, 2958. <https://doi.org/10.3390/su15042958>

Academic Editor: Pablo García Triviño

Received: 21 December 2022

Revised: 1 February 2023

Accepted: 2 February 2023

Published: 6 February 2023



Copyright: © 2023 by the authors. Licensee MDPI, Basel, Switzerland. This article is an open access article distributed under the terms and conditions of the Creative Commons Attribution (CC BY) license (<https://creativecommons.org/licenses/by/4.0/>).

1. Introduction

With the shortage of energy and the increasing problem of environmental pollution, distributed energy has gradually come into people's view, and the energy internet (EI), with electricity at its core, has come to be paid more attention [1,2]. The energy router (ER) is the core equipment for energy internet architecture, effectively integrating distributed energy sources, realizing AC–DC free conversion and multi-directional flow of energy, and effectively reducing the impact brought about by distributed energy sources and AC–DC load access to the power system [3–5], and the popular use of energy routers is an essential trend for the future development of the energy internet. For interconnected systems of distributed energy sources, a reasonable energy router architecture, suitable energy scheduling and coordination control strategy are the key factors for determining the stable operation of the system [6,7]. ER can not only solve the problem of distributed energy grid connection, but also provide a plug-and-play interface for different devices. ER can achieve the goal of power system control integration. Therefore, research on ER is very urgent.

Depending on the demand and the location, energy routers with different classifications are also used, and can mainly be divided into terminal energy routers, regional energy routers, and backbone energy routers [8–10]. Normally, energy routers applied to the backbone and area are relatively mature, while those applied to the terminal have been less thoroughly researched. Energy routers for terminal applications are widely used,

and can effectively utilize distributed energy and meet the development goal of “double carbon”, having high research significance.

Therefore, energy routers have accordingly been studied in terms of overall architecture [11], control strategy [12,13], internal communication design [14], and key parameters [15], but so far, no expert scholars have proposed a general energy router architecture and a control strategy that can satisfy various operating conditions. Ref. [16] proposed a coordinated control strategy for AC–DC hybrid ER based on energy storage and voltage stabilization that used multiple sets of converters to provide a wealth of AC–DC ports, and also classified the external ports for consideration, but its module control strategy was relatively simple, and the dynamic performance required improvement. Ref. [17] proposed a multi-LAN port energy router that could easily connect distributed power sources and AC–DC loads to the backbone grid, but did not consider the access of energy storage systems, and the energy router architecture was not complete. Ref. [18] provided the design idea of a community energy router, giving different operating states of the energy router under distribution network failure. However, no specific feasible topology was given. In [19], a power allocation strategy for seamless switching conditions was proposed, but it lacked precise consideration of the battery. In [20], a two-level modular ER structure that could be applied to DC microgrid clusters was proposed to realize the function of flexible interconnection of microgrids. In [21], the impact on the energy router under grid fault conditions and the balancing strategy of the capacitor voltage under various conditions were analyzed, but only situations under single-phase grid faults were considered, without considering two-phase or multiple three-phase faults.

The study of ER is at this stage no longer limited to the ER itself, as the grid-connected port is connected to the distribution grid. Therefore, research on the power quality of the distribution grid port and the energy allocation and optimization of the distribution grid side is also meaningful. In ref. [22], the authors proposed a hierarchical grid model to enhance the resilience of DC-MGs. In refs. [23,24], the researchers studied energy hubs. These include wind power, solar power, and energy storage. The management of distributed energy sources and the improvement of distribution network reliability, respectively, were studied. However, these papers are all macroscopic studies, but do not explain the details of ER.

Due to the nature of the energy router, the presence of a grid-connected port is necessary. When the energy router is connected to the grid, if it is not established with a battery or the battery is not properly controlled and directly connected to the grid, it will result in high network loss. The battery is able to play the role of a bridge for energy circulation, carry out energy buffering, and can also help the energy router to stabilize the bus voltage. For the regulation of the energy router, the use of the battery, the state of charge of the battery, and the comprehensive deployment of the battery discharge power also need to be considered [25–28]. Refs. [29,30] mention a variety of optimization algorithms that serve as a theoretical basis for the future expansion of ER and its integration with power systems, and the future expansion of power systems will be studied in depth on the basis of the algorithms. Refs. [31,32] propose optimization algorithms in combination with biology, and these algorithms are better able to optimize the energy allocation strategy of energy routers and improve their efficiency.

On the basis of the existing research, the study of ER has primarily focused on structure as well as on control. Therefore, in this paper, we design a five-port energy router topology in consideration of these two points and propose a corresponding control strategy for this structure.

The first point is the design of the topology. In accordance with the requirements, an ER including PV, energy storage, grid-connected, AC, and DC ports was proposed. All ports are connected by a DC bus, and are unified and controlled by a central processor. The topologies of different ports are designed to realize the energy flow.

The second point is the implementation of the control strategy. The control strategy is divided into two layers, which are the independent control of the ports and the overall

coordinated control. For the port functions, each port designs an independent control strategy to maintain stability. At the same time, the top-level control is designed to divide the working modes, and the different ports operate in a coordinated fashion under different working modes to finally work stably.

2. Energy Router Topology Creation and Analysis

In the original model, the ER system integrates the PV, the AC load, and the DC load. In response to the need to provide various ports involved in energy routers, this paper proposes a five-port energy router for a wide range of applications. The router architecture is shown in Figure 1, and the five groups of ports are the PV port, the energy storage port, the grid-connected port, the DC load port, and the AC load port. All ports of the energy router converge into a DC common bus (CB), and U_{CB} is the common bus voltage. $i_1 \sim i_5$ are the output current values of the five ports, which can represent the interaction with the common bus energy handover.

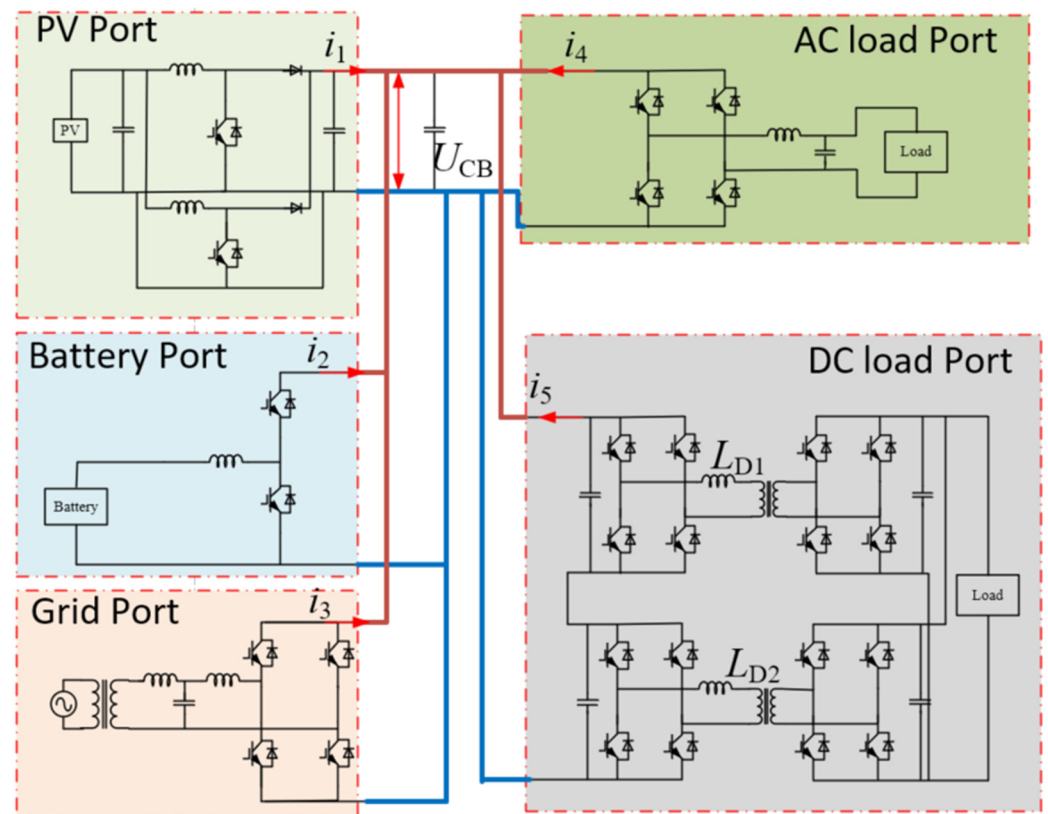


Figure 1. The architecture of five-port ER.

Port 1 is the PV port structure, considering the low voltage level of solar power (PV) and the high voltage level of the common bus, the boost topology is used, and considering the switching tube current stress and ripple, this port adopts the interleaved parallel boost structure. i_1 is the PV port and common bus interaction current, the PV port and common bus interaction power $P_1 = i_1 U_{CB}$, for the energy storage port, the adopted structure is a two-level converter; i_2 is the storage port, and the common bus current storage port interaction power $P_2 = i_2 U_{CB}$, where the port plays the role of stabilizing the DC bus voltage. For the grid-connected port, the structure of a two-level converter combined with an LCL filter is used, which is connected to the grid to realize the interaction of energy with the grid, and the interaction power is $P_3 = i_3 U_{CB}$, for the AC load port, the structure of a two-level converter and an LC filter is used, and the interaction power with the common bus is $P_4 = i_4 U_{CB}$; for the DC load port, a parallel input structure is used. For the DC load

port, the structure used is an input parallel-type double active bridge converter (ISOP DAB), and the interaction power of the port with the common bus is $P_5 = i_5 U_{CB}$.

The system has a total of five groups of ports, ignoring port losses, and the real-time power balance of the system using the common bus is shown below.

$$P_1 \Delta t + P_2 \Delta t + P_3 \Delta t + P_4 \Delta t + P_5 \Delta t + P_{non} \Delta t = 0 \quad (1)$$

$$P_{non} \Delta t = \frac{1}{2} C_{CB} U_{CB}^2 \quad (2)$$

$$\sum_{k=1}^5 i_k U_{CB} + \frac{1}{2} C_{CB} U_{CB}^2 = 0 \quad (3)$$

where U_{CB} is the current common bus voltage value, C_{CB} is the DC bus capacitance value, i_k is the interaction power generated by each port with the DC bus, and P_{non} is the unbalanced power of the system at the current moment. Due to the changes in PV, load, etc., fluctuations in P_{non} will be caused, and will be accompanied by fluctuations in U_{CB} . Therefore, the overall coordination control starts from the stable control of U_{CB} , and stable operation of the system is finally realized by controlling the energy interaction status of the energy storage port and the grid-connected port with the main line.

For the energy router, the five groups of ports involved are divided into two parts, consisting of the functional port, for the unidirectional flow of energy, and the voltage stabilization port, for the bidirectional flow of energy. Among them, the PV, AC and DC load ports are the functional ports, and the grid-connected energy storage ports are the voltage stabilization ports.

The structural design of the PV port adopts the structure presented in Figure 2.

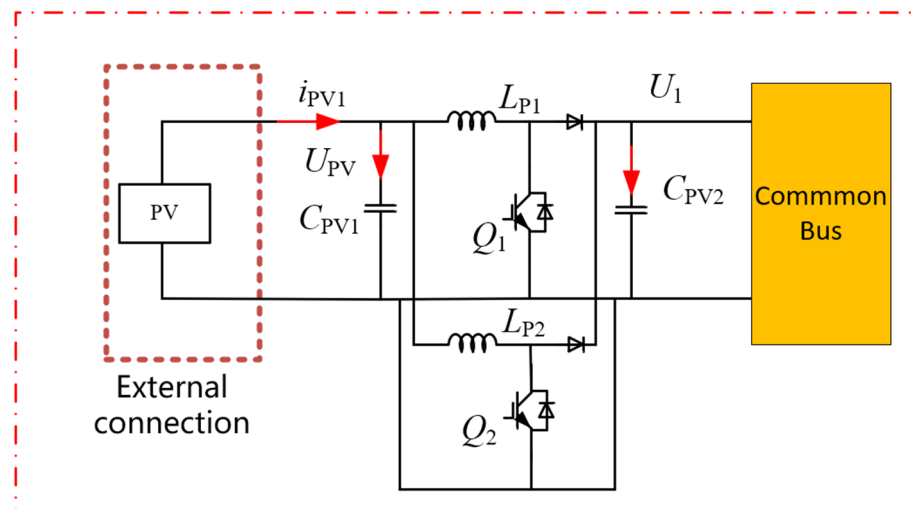


Figure 2. The architecture of the PV port.

The function of the PV port is to incorporate solar energy into the energy router system, and the criterion of its work is the full utilization of light energy without considering factors such as energy flow system stability, so the design and control of the PV port start from the efficient acquisition of energy without involving other factors. Considering the characteristics of low PV voltage level, multiple parallel PV cells, and high DC bus voltage level, a boost converter is used as the port, and considering the expandability and the current stress of the switching devices, the boost converter structure adopts an interleaved parallel boost circuit. When the power is the same, the current stress of the staggered parallel booster structure switch tube is lower than that of the ordinary booster circuit; the current ripple is also smaller, which is advantageous for the stability of the common bus voltage and current control.

For the design of the AC load port, considering the controllability of the system and the overall control difficulty, the AC port is not involved in internal voltage stabilization, and is only used as a functional port to supply the load, so the control method and basic structure are the same as those of the conventional inverter. It is sufficient to ensure the output stability and realize the basic external functions. Figure 3 shows the topology of the AC load port, with the output connected to the outside through an LC filter.

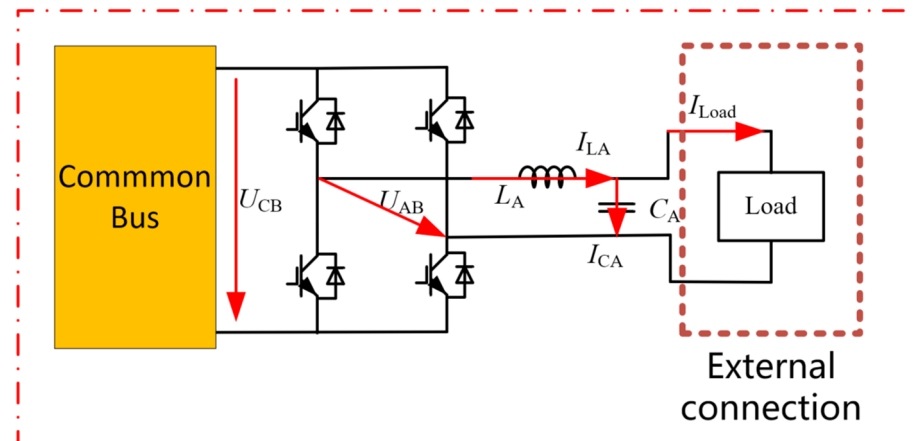


Figure 3. Topology of AC load port.

For the DC port shown in Figure 4, the overall situation is similar to that of the AC port, which is also only used as a functional port to provide DC output without participating in system regulation, and only needs to ensure output stability and achieve basic functions. Considering the widespread use of electric vehicles, the DC port usually needs to provide a greater amount of power, and in terms of electrical isolation, the output of the two modules is connected in series with the output of the parallel-type double active bridge converter (ISOP DAB) to realize the external connection. This structure can effectively increase the output power and reduce the device's current stress.

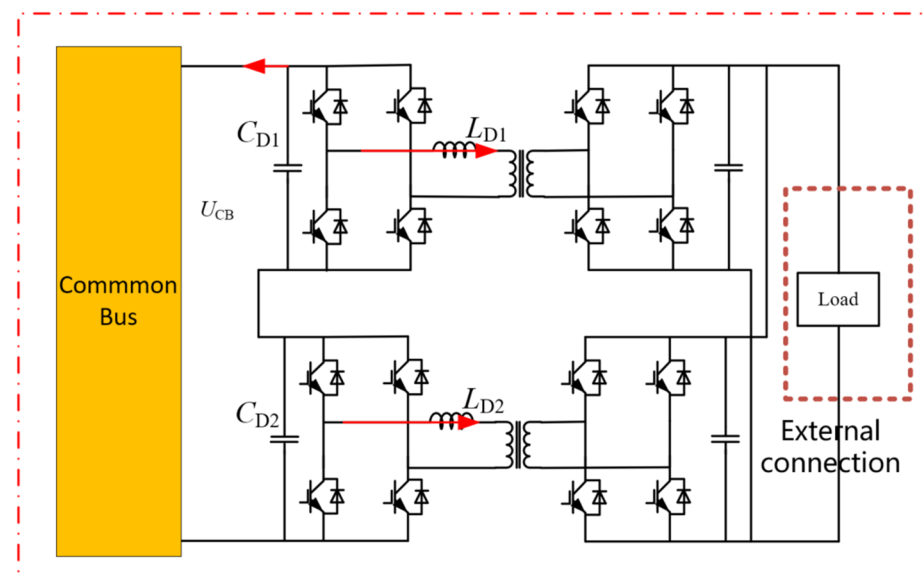


Figure 4. Topology of the DC load port.

For a two-module ISOP-type DAB structure, as described in Figure 5, the modules at the input are voltage-divided, and the voltage at the output is automatically equalized. Due to the manufacturing process, the parameters between the modules are not exactly the

same, and the power balance between the modules needs to be considered. When the input voltage equalization loop is in stable operation, the system achieves power equalization among modules and current equalization at the output with $I_{21} = I_{22}$. When the input voltage of the system is disturbed, the input voltage equalization loop can be controlled so that the input voltage of each module receives equalized control. When the output current of the module is disturbed and increases, the output voltage of the module decreases, because the input voltage equalization loop has already achieved system power balance.

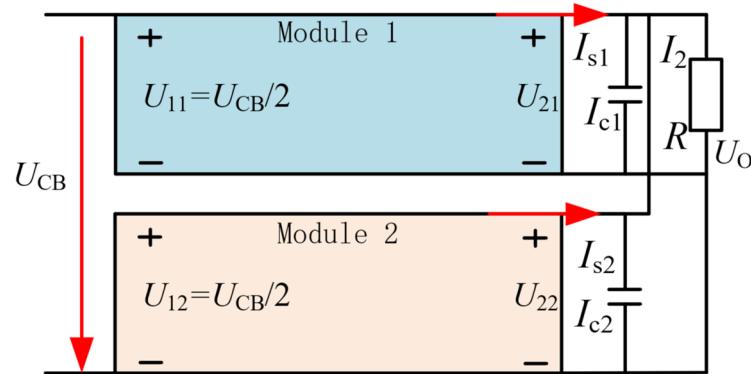


Figure 5. Equivalent diagram of ISOP DAB converter.

The output voltage drop leads to the current flowing to the load becoming smaller and the current flowing to the inductor becoming larger, at which time the inductor is charged and the voltage increases, forming negative feedback regulation, and the system output voltage restores a stable value again. As can be observed, the input voltage equalization loop can simultaneously control the system input voltage waveform and the system output current fluctuation, and ensure the power balance between the system modules from the input side and the output side at the same time.

The grid-connected port is different from the two load ports and the PV port in that it assumes the function of bidirectional energy flow, and is thus an important structure for realizing the energy routing function by obtaining energy from the grid to provide loads when the system energy is insufficient and feeding the excess energy back to the grid when the system energy is excessive. For the grid-connected ports, the structure used is the single-phase rectifier structure shown in Figure 6.

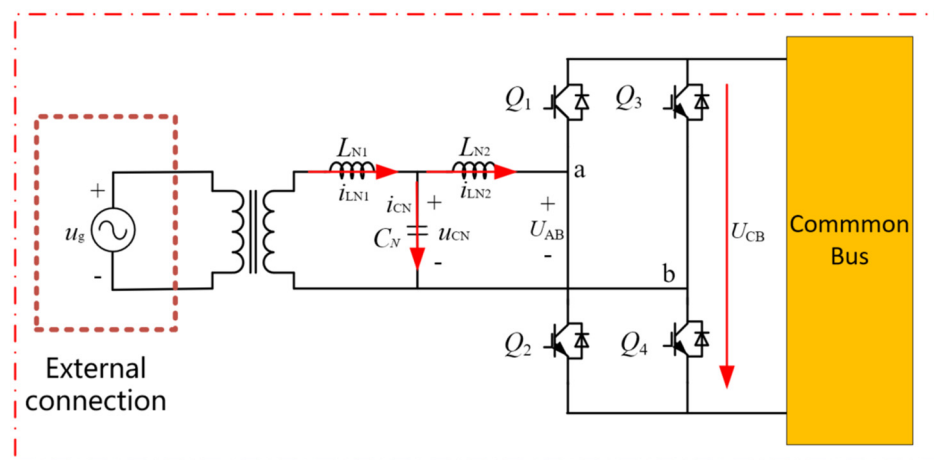


Figure 6. Topology of the grid-connected port.

The grid-connected port is connected to the grid through a set of LCL filters. As a third-order system, LCL filters are small in size and have good high-frequency filtering

performance, but the structure has resonant peaks, which can reduce the stability of the system. In the control, the resonant peaks are suppressed by adding virtual resistors.

The energy storage port plays the role of stabilizing the DC bus voltage, connecting the battery, and buffering the energy, and is the most critical port in terms of the control of the energy router. This port needs to realize the bidirectional flow of energy, and also requires rapid control that is able to quickly sense the fluctuation of the common bus voltage and make adjustments in the control. Therefore, a bidirectional buck–boost structure, as shown in Figure 7, was chosen, and its control adopts the faster model predictive control.

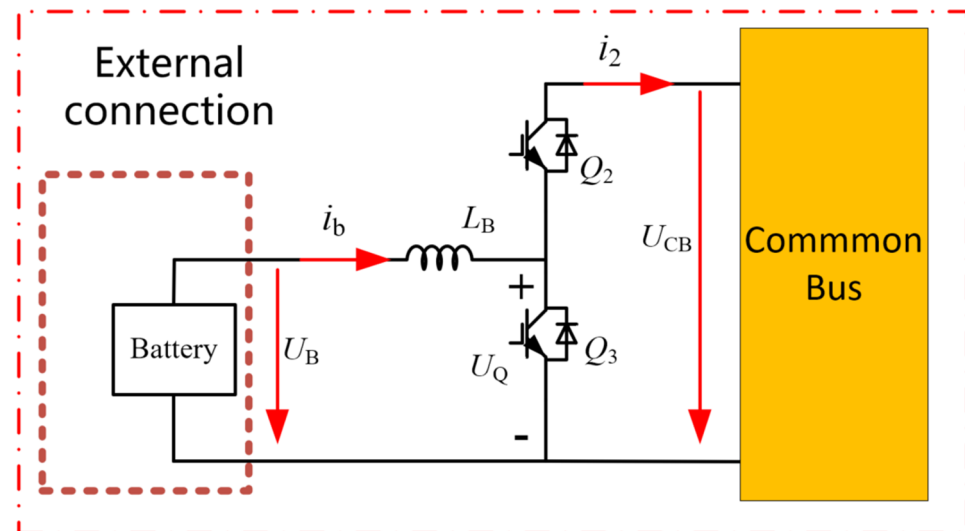


Figure 7. Structure of the energy storage part.

The port realizes the bidirectional flow of energy by controlling the opening and closing of switch tubes Q_2 and Q_3 . When Q_3 is cut off, the opening and closing of Q_2 are controlled, meaning that the circuit works in the boost mode, whereby energy is transferred from the battery to the DC bus. When Q_2 is cut off, the opening and closing of Q_3 are controlled, and the circuit works in the buck mode, whereby energy is transferred from the DC bus to the battery, thus realizing the bidirectional flow of energy.

An overview of the energy flow directions and functions of the five ports is provided in Table 1. Obviously, the energy of the first two ports flows in both directions, and the functions are more complex and have more important positions. The last three ports only function to perform energy transfer, and do not play a dominant role in the control.

Table 1. ER ports and functional description.

Port	Direction of Energy Flow	Function
Battery Port	Bidirectional	1. Coordinated energy flow 2. Stabilize UCB 3. Coordinated energy storage batteries
Grid port	Bidirectional	1. Coordinated energy flow 2. Stabilize UCB 3. Integrating ER with the grid
PV Port	Unidirectional external to ER	Transferring solar energy to the ER.
AC load port	Unidirectional ER to external	Provide power for AC load
DC load port	Unidirectional ER to external	Provide power for the DC load

3. Energy Router Control Strategy Research

3.1. Overall Control Architecture and Control Strategy

For the control of the energy router, the most effective current is achieved using the hierarchical control strategy; in this control strategy, the port controller performs control using local information, and on this basis maintains two-way contact with the central controller. The control architecture is shown in Figure 8, where the overall control architecture is divided into four layers, comprising (from top to bottom) the top-level control platform, the information collection platform, decision control and the bottom-level control platform. Information enters the controller at the bottom and flows upwards, and control signals enter the port at the top and flow downwards.

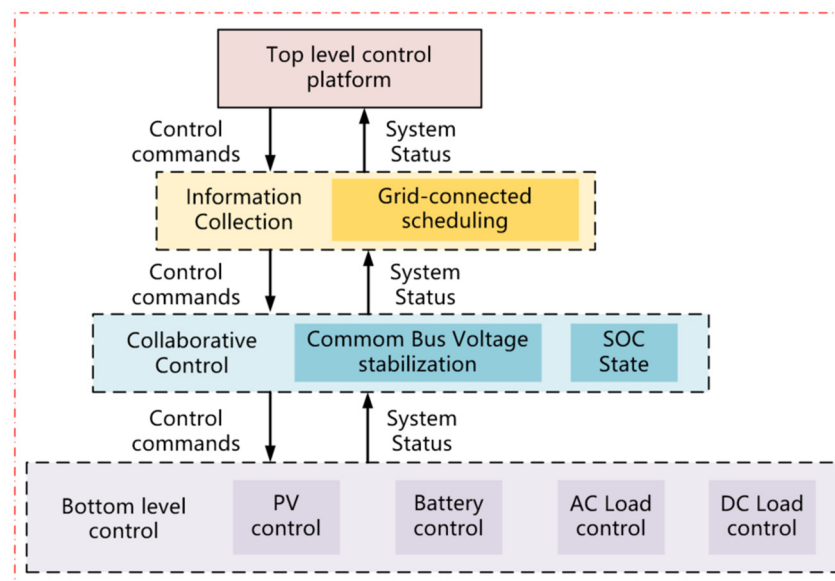


Figure 8. Hierarchical control architecture of five-port ER.

For the proposed five-port energy router topology and the hierarchical control architecture used in this paper, the bottom-level control layer and the cooperative control layer are the core of the study. The bottom-level control layer corresponds to the independent control of the five ports, and the cooperative control performs overall control of the ports' operating states by means of bus voltage and battery charge state. The cooperative control layer includes two points, bus voltage stabilization and battery charge state adjustment, both of which are closely related to the energy storage ports. Therefore, this study focuses on the energy storage port in the design and control of the bottom-level port, and establishes an overall control strategy for the port that is able to realize reasonable control of the bus voltage and stability, as well as the battery charge state, so as to finally realize the free flow among multiple energy sources and the stable operation of the energy router. The energy router works stably.

3.2. Five-Port Control Strategy Design

The first is the control of the PV port, which is a unidirectional functional port, and its control goal is to inject as much light energy as possible into the common bus. For this system, in order to ensure that the load attains maximum power, proper load matching is required. When the load resistance is equal to the internal resistance of the power supply system, the load receives the maximum power, with such a load matching process being referred to as maximum power point tracking (MPPT) [33,34]. Figure 9 shows the process of MPPT for the PV port. By collecting the power at the current moment and comparing it with the power at the previous moment, the switching tubes are controlled by judging the change in power, while using a staggered parallel boost structure, where the control

signals of the two groups of switching tubes are the same, but the delta carrier signals are staggered by half a cycle to achieve harmonic offset.

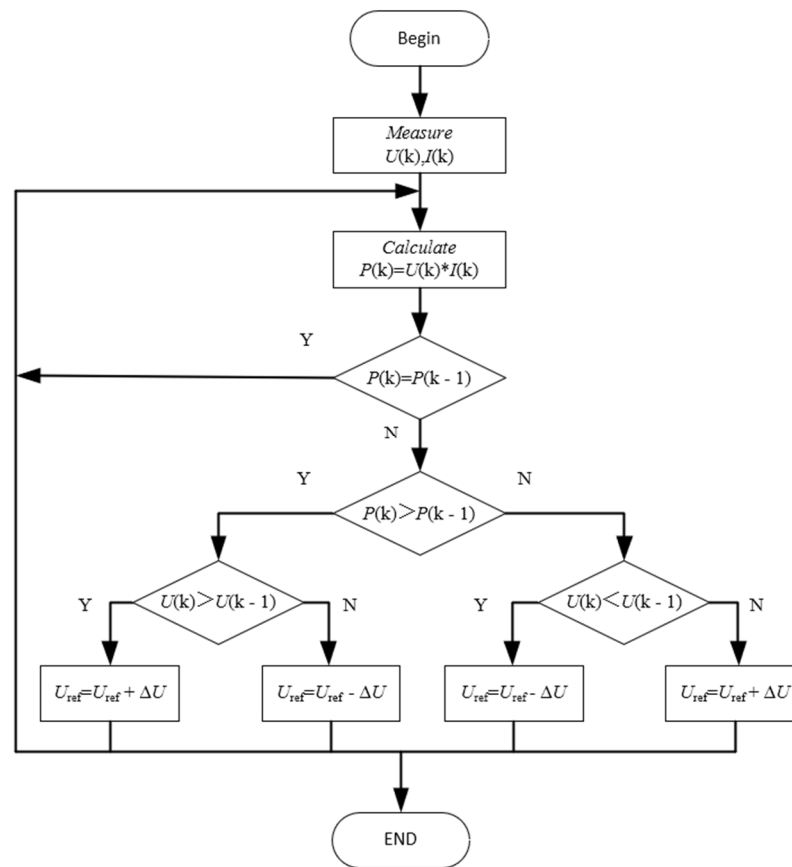


Figure 9. PV module structure and control block diagram.

For the AC load port, as can be seen from the structure topology diagram in Figure 3, the output is connected to the load using an LC filter. It is not a bad idea to set the load as a resistive load with resistance R . Then, in the complex frequency domain, we have:

$$\begin{cases} I_{LA}(s) = \frac{U_{AB}(s) - U_c(s)}{L_A s} \\ (I_{L1}(s) - I_{Load}(s)) \frac{1}{C_s} = U_c(s) \\ I_{Load}(s) = \frac{U_c(s)}{R} \end{cases} \quad (4)$$

Using bipolar SPWM modulation, in one switching cycle:

$$\overline{U_{AB}} = (2D - 1)U_{CB} \quad (5)$$

$$D = \frac{1}{2} \left(1 + \frac{V_m}{V_{tri}} \right) \quad (6)$$

where D is the duty cycle, V_m is the reference sine wave, which is the input to the modulator, and V_{tri} is the peak delta carrier wave.

$$\overline{U_{ab}} = (2D - 1)U_{CB} \quad (7)$$

$$\overline{U_{ab}} = \left[2 \times \frac{1}{2} \left(1 + \frac{V_m}{V_{tri}} \right) - 1 \right] U_{CB} = \frac{V_m}{V_{tri}} U_{CB} \quad (8)$$

Then, the transfer function of the AC port can be obtained as follows:

$$G_0(s) = \frac{U_0(s)}{V_m(s)} = \frac{1}{L_A C s^2 + \frac{L_A}{R} s + 1} \frac{U_{CB}}{V_{tri}} \tag{9}$$

For the AC load port, a dual closed-loop voltage and current control are used, and the control strategy is shown in Figure 10.

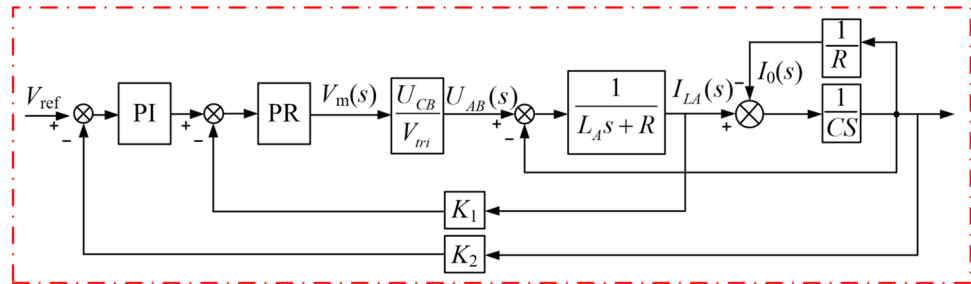


Figure 10. AC load port control structure diagram.

The voltage outer loop is the error signal obtained by comparing the reference value with the sampled value of the output voltage, and then the current reference value of the inner loop is generated by the PI controller; the current reference value of the inner loop and the inductor current obtained from the actual sampling are used to generate the current error, and the modulated wave is obtained from the proportional resonance of the inner loop. The feedforward of the reference value is also added to improve the time response characteristics.

For the DC port, an ISOP DAB topology is used, as shown in Figure 4. For this structure, a centralized dual-loop voltage equalization control strategy is used, which is based on the principle whereby a voltage loop is used to control the output voltage, and an independent input voltage loop is used to equalize the input voltage. When the input voltage of a module in the system is disturbed and increases, it can be seen from Figure 11 that the offset control amount of the module also increases, so the output phase shift duty cycle increases, the output power increases, the system input side capacitor is in a discharged state, and the voltage drops, thus stabilizing the output voltage [35].

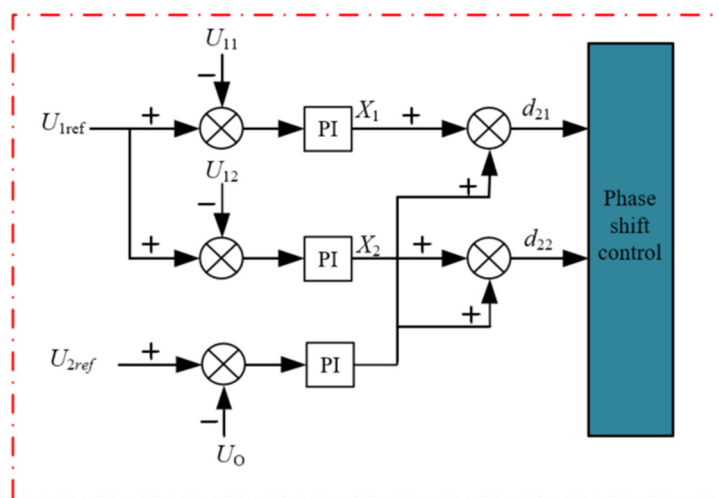


Figure 11. Block diagram of the double-loop voltage equalization control system for DAB.

For the grid-connected port, a single-phase rectifier structure is used, as shown in Figure 6: the grid side and the LCL filter and rectifier are isolated using a transformer, and the LCL filter circuit is connected to the DC bus side using the single-phase rectifier.

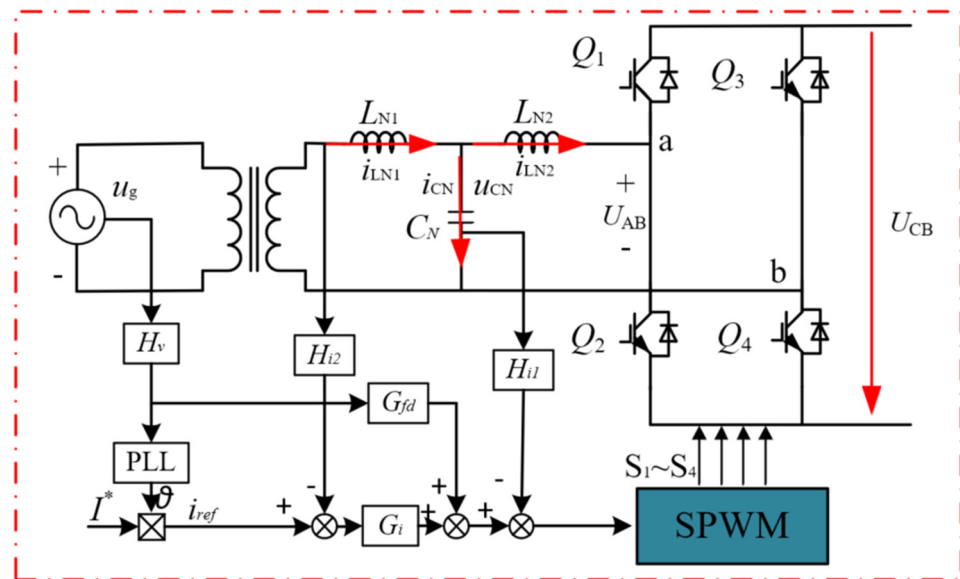


Figure 13. Control block diagram of the structure of the grid-connected port.

As can be observed from the energy storage port structure diagram depicted in Figure 7,

$$U_Q = L_B \frac{di_b}{dt} + U_b \tag{12}$$

Using a discretized form, the transformation of Equation (7) yields

$$i_L(k+1) = (U_Q - U_b) \frac{T_s}{L_B} + i_L(k) \tag{13}$$

Using the sensor, we can get i_l at moment K . On the basis of prediction, we can get i_{lK+1} . Let's assume that the converter is working in the buck mode at this time; then, we have

$$i_L(k+1) = (DU_{CB} - U_B) \frac{T_s}{L_B} + i_L(k) \tag{14}$$

Usually, for digital control systems, there is a certain delay time, which is expressed as follows:

$$i_L(k+1) = (D_{old}U_{CB} - U_B) \frac{T_s}{L} + i_L(k) \tag{15}$$

where D_{old} is the duty cycle of the previous moment. Generally, a constant voltage is considered for a given sampling period; therefore, we have

$$D = \frac{(i_{L_ref} - i_L(k+1))L}{T_s U_{CB}} + \frac{U_B}{U_{CB}} \tag{16}$$

The block diagram of the energy storage converter control is shown in Figure 14. First, the U_{CB} and the given reference voltage U_{CB_ref} are sent to the proportional-integral PI for comparison, at which time a reference current is output for comparison with the actual inductor current and sent to the model predictive controller in order to generate the duty cycle, and the output is compared with the carrier waveform to generate the control signal. When the bus voltage fluctuates, it can be adjusted by this model predictive control strategy.

storage port receives energy from the bus, and the grid-connected port does not participate in the work.

Table 2. The working model of ER.

Model	U_{CB}	SOC	Illumination	Model
Model A	$U_{CB} < U_{CB_ref}$	SOC < 20%	Sufficient	Model 1
Model A	$U_{CB} > U_{CB_ref}$	SOC < 20%	Sufficient	Model 2
Model B	$U_{CB} < U_{CB_ref}$	SOC < 20%	Insufficient	Model 3
Model B	$U_{CB} > U_{CB_ref}$	SOC < 20%	Insufficient	Model 4
Model C	$U_{CB} < U_{CB_ref}$	SOC > 80%	Sufficient	Model 5
Model C	$U_{CB} > U_{CB_ref}$	SOC > 80%	Sufficient	Model 6
Model D	$U_{CB} < U_{CB_ref}$	SOC > 80%	Insufficient	Model 7
Model D	$U_{CB} > U_{CB_ref}$	SOC > 80%	Insufficient	Model 8
Model Z	$U_{CB} < U_{CB_ref}$	20% < SOC < 80%	Sufficient	Model 9
Model Z	$U_{CB} > U_{CB_ref}$	20% < SOC < 80%	Sufficient	Model 10
Model Z	$U_{CB} < U_{CB_ref}$	20% < SOC < 80%	Insufficient	Model 11
Model Z	$U_{CB} > U_{CB_ref}$	20% < SOC < 80%	Insufficient	Model 12

Model B is the “grid-connected charging model”, where the energy router storage port is “non-stocked” and the PV is insufficient, and it is necessary to get energy from the grid to meet the requirements of load consumption.

Model C is a “grid-connected power generation model”, where the energy router is full of energy storage and the PV is sufficient to feed the acquired energy back to the grid.

Model D is an “off-grid discharge model”, where the energy router has sufficient energy storage and the PV is insufficient, and the energy router supplies the AC/DC port consumption from its own energy storage.

Model Z is the “intermediate model”, which is the middle model among Models A–D, indicating that the energy router is self-sufficient and works normally, and this intermediate state is off grid, which is the ideal working state, and the energy router is regarded as a “micro grid” without an external connection. The energy is generated and consumed by the system itself, without any interaction with the outside world.

The five-port energy router transitions between the above five working models, and the different working models represent the different working states of the energy storage and grid-connected ports, thus realizing the stable overall control.

4. Simulation Verification and Analysis

In order to verify that the energy router topology proposed in this paper and the corresponding control strategy are feasible, an energy router model based on model predictive control was built using the MATLAB/Simulink platform, and its main parameter settings are shown in Table 3.

Considering the battery storage state and the limitation of simulation time, the initial storage value of the battery, SOC, in the energy router “Model Z” was set to 60%, and its range was set to $59.993 < \text{SOC} < 60.009$. The initial light intensity of the simulation was set to 1000 w/m^2 , and the output power of the PV port was about 10 kW at this time. The initial light intensity of the simulation was set to 1000 w/m^2 , and the output power of the PV port was about 10 kW at this time. The light dropped at 1.1 s and then dreopped again to 0 at 1.3 s, after which the PV port stops working.

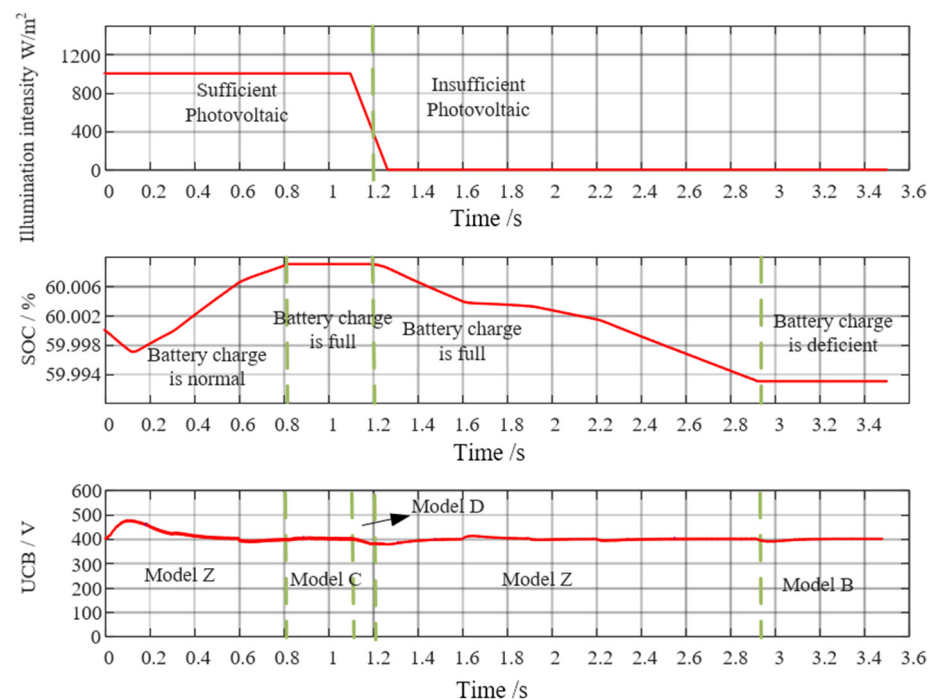
The system functional port states are as follows: the initial state is set to have only the AC port working, the load power is about 1 kW, and the initial working model of the system is the Z-intermediate model. The system puts the DC port into operation at 0.6 s, the light starts to drop at 1.1 s, and decreases to 0 at 1.3 s, the DC load port < at 1.6 s, the AC port increases the load at 1.9 s, and the load further increases at the AC port at 2.2 s.

Table 3. Parameters of ER.

Parameters	Value
Common Bus voltage U_{CB_ref}	400 V
PV port inductors L_{P1}, L_{P2}	5 mH
PV module open circuit voltage	309 V
PV port capacitor C_{P1}	3300 μ F
Energy storage inductor L_B	5 mH
Grid port inductor L_{N1}	0.6 mH
Grid port inductor L_{N2}	0.2 mH
Grid port capacitor C_N	10 μ F
AC load port inductor L_A	5 mH
AC load port capacitor C_A	6 μ F
DC load inductor L_{D1}	50 mH
DC load inductor L_{D2}	47 mH
DC load capacitor C_{D1}	470 μ F
DC load capacitor C_{D2}	500 μ F
Initial light intensity I_0	1 kW/m ²
Initial SOC	60%

The system voltage regulator ports work as follows: 0–0.8 s, only the energy storage port works, and the battery is charged; 0.8–1.2 s, the grid-connected port works and outputs energy to the grid; 1.2–2.9 s, the energy storage port works, and the battery is discharged. Then, 2.9 s later, the grid-connected port works, and obtaining energy from the grid.

The light intensity, battery SOC, and common bus voltage U_{CB} waveforms are plotted in Figure 16. The plot characterizes the expected battery storage state with the change in external model change and the throwing of AC and DC loads, with the common bus changing with the load.

**Figure 16.** Lighting intensity, energy storage, common bus voltage.

As can be seen in Figure 16, the simulation is started, and the system is in model Z at 0–0.8 s. At 0.8 s, the animal battery is fully charged, and the system enters model C. At 1.1 s, the PV drops to 0, and the system enters model D. The system stabilizes and re-enters model Z. The battery SOC drops further until the system enters model C at 2.9 s.

Different model switching methods correspond to different converter operating states, and the steady-state operation of the energy router can be observed on the basis of the DC bus voltage, which fluctuates with load switching and model change, but can be stabilized quickly.

Figure 17 shows the PV port power curve, which reaches the light inflection point at 1.1 s, after which the PV power gradually decreases to 0, which is consistent with the light situation in Figure 16, and the PV port works normally.

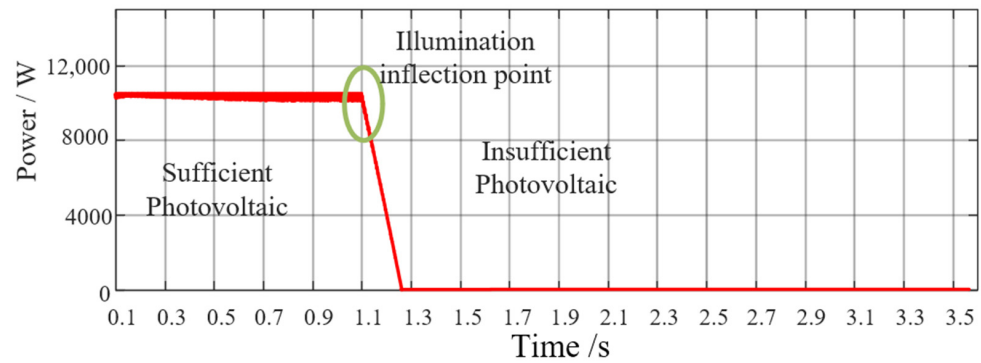


Figure 17. PV port power curve.

Figure 18 shows the power fluctuation of the AC and DC load ports and the bus voltage fluctuation. The four graphs represent the AC port load power, DC port load power, total load power, and the fluctuation of bus voltage when the load is switched. The AC load increases from 1 kW to 3 kW to 5 kW, and its output power is rapidly stabilized, while the DC load increases from 0 to 5 kW and then decreases. From the power fluctuation graph and the DC bus voltage fluctuation graph, it can be seen that the AC and DC load ports are able to realize basic functions, and the bus voltage can quickly return to stability when the AC and DC loads are added and removed.

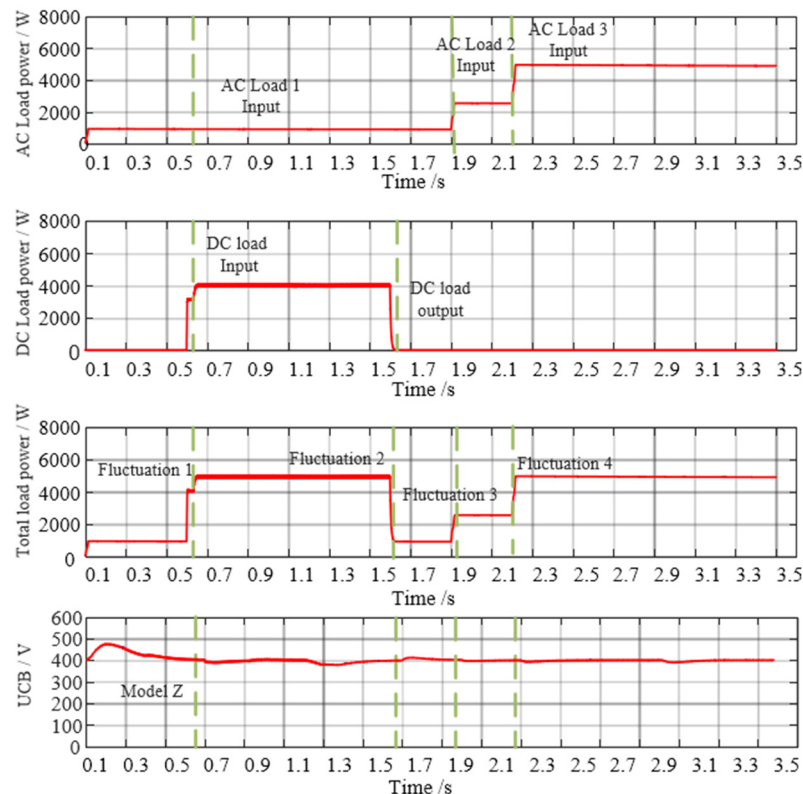


Figure 18. Power fluctuation and common bus voltage diagram.

Figure 19 shows the voltage and current power of the grid-connected port of the energy router; there is no energy exchange at the power port before 0.8 s, and at 0.8 s, the power port delivers energy to the grid, corresponding to model C in Figure 14; the corresponding battery is full of electricity, and the PV port continues to generate energy, at which time the excess energy is fed back to the grid. At 1.1 s, the PV exits, and the AC/DC port is supplied with energy from the battery, at which point the grid-connected port stops working. At 2.9 s, the storage port stops working, and the load continues to consume energy, at which point it enters model B. The grid-connected port receives energy from the grid in order to provide the required load for consumption.

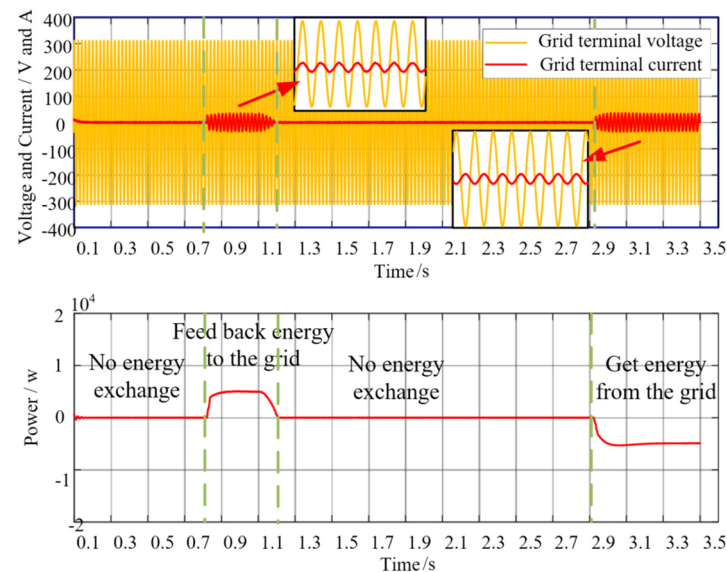


Figure 19. Voltage, current and power diagram of grid-connected port.

Figure 20 shows the voltage at the input of the ISOP DAB and the division of the CD1, CD2, and DC load voltage is implemented at 0.6 s. Due to the different input parameters of the ISOP DAB, the voltage division at the input is different. Under the double closed-loop voltage division control designed as shown in Figure 11, the two sets of input voltages are rapidly equalized, while at the same time, due to the change in the model, it is possible to satisfactorily follow the voltage at the input.

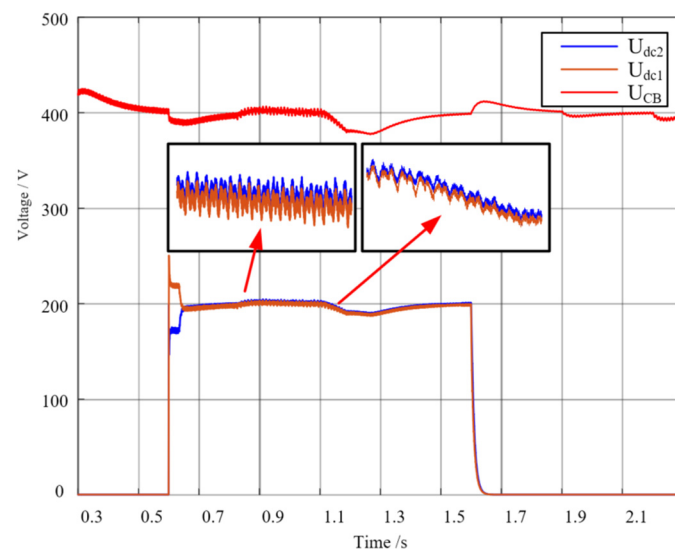


Figure 20. Capacitive voltage at the DAB input.

Figure 21 presents a spectral analysis of the grid-connected port, where the harmonic distortion rate is only 3.02%. Using the energy router topology and the corresponding control method proposed in this paper, the output current waveform is good, and the impact on the grid is small.

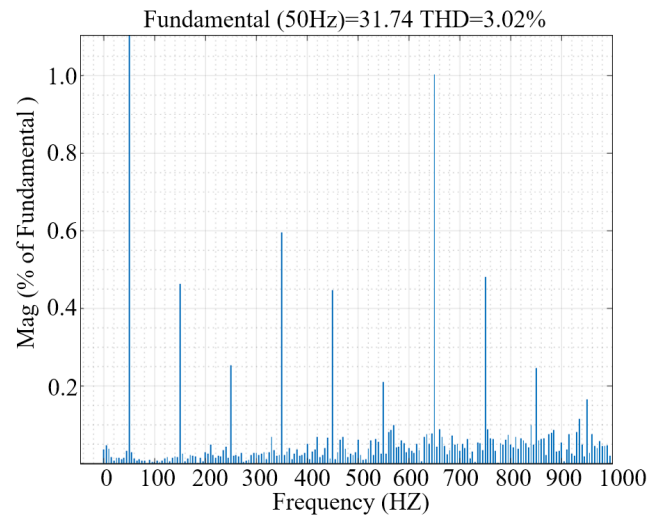


Figure 21. Spectral analysis of the grid-connected port.

The study of ERs is divided into analysis at the module level and at the system level. The study in this article also starts from these two levels.

As shown in Table 1, at the module level, the system is divided into five ports. The first port is the energy storage port. As shown in Table 1, the functions of the energy storage port are divided into three parts. These three functions are verified in Figure 16. Figure 16 shows the change in the SOC of the energy storage port and the corresponding change in the ER operating mode. The second is the grid-connected port, as shown in Table 1, the functions of which can be divided into three parts. These functions are demonstrated in Figure 19, as well as in Figure 21. Figure 19 shows the direction of energy flow in the grid-connected port and the role played by the energy storage port in stabilizing the bus voltage. From Figure 21, it can be observed that the grid-connected port not only fulfills the function of energy coordination, but also has less impact on the distribution network. The third is the photovoltaic port; Figures 16 and 17 show the functionality of the photovoltaic port with different current light intensities and different levels of output power. Finally, there are two load ports, and Figure 18 shows the stability of the system when the two load ports are working in alternation.

System-level studies are effectively equivalent to all ports working in coordination, with energy flowing freely and on demand. All ports are able to work properly throughout this process, thus reflecting the stable operation of the system.

Figure 22 shows the working status of different ports at different points in time, as well as the coordinated work of all ports, which makes it possible to finally realize the free flow of energy.

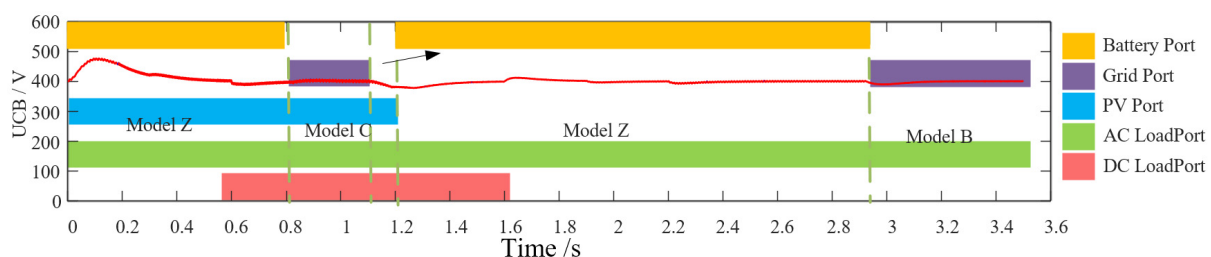


Figure 22. Model switching and port coordination diagram.

5. Conclusions

In this paper, a five-port energy router topology was designed on the basis of the basic function of the energy router, where the five external groups of ports correspond to the five groups of topologies, and a corresponding control strategy is designed for each port. At the same time, an energy router model switching strategy was designed according to the flow of energy and the storage of that state. Through the switching of different models, the external state changes can be satisfied, while stability is achieved for the voltage of the bottom bus. The feasibility of this energy router was subsequently verified. Compared with previous studies, the innovations presented in this study are as follows:

- (1) At the module control level, model predictive control was applied to the module control of ER, resulting in the common bus voltage having a faster stabilization speed. At the module topology level, for high-power modules, such as photovoltaic modules, a staggered parallel structure was used in order to reduce the current stress and improve feasibility. Finally, a reasonable and feasible five-port topology and control structure was designed.
- (2) A corresponding modal division strategy was proposed for the internal energy storage state and energy flow direction of the energy router, and through the division of this strategy, reasonable control of the energy storage port and the grid-connected port is realized, and the effective switching of the working modalities reflects the characteristics of the interactive flow of energy, which has a certain practical value in engineering applications.

Author Contributions: Conceptualization, X.C., Y.L., D.Y., T.J. and M.A.M.; Methodology, X.C., Y.L., D.Y., T.J. and M.A.M.; Software, X.C. and Y.L.; Validation, X.C., D.Y., T.J. and M.A.M.; Formal analysis, M.A.M.; Investigation, D.Y. and T.J.; Writing—original draft, X.C., Y.L., T.J. and M.A.M.; Writing—review and editing, X.C., Y.L., D.Y., T.J. and M.A.M.; Supervision, T.J. and M.A.M. All authors have read and agreed to the published version of the manuscript.

Funding: This work was supported by the Chinese National Natural Science Foundation (grant number 51977039) and the central government guiding local science and technology development project under grant number 2021L3005.

Data Availability Statement: Not applicable.

Conflicts of Interest: The authors declare no conflict of interest.

References

1. Huang, A.Q.; Crow, M.L.; Heydt, G.T.; Zheng, J.P.; Dale, S.J. The Future Renewable Electric Energy Delivery and Management (FREEDM) System: The Energy Internet. *Proc. IEEE* **2010**, *99*, 133–148. [[CrossRef](#)]
2. Wen, J.; Zhou, B.; Wei, L. Preliminary study on an energy storage grid for future power system in China. *Power Syst. Prot. Control* **2022**, *50*, 1–10.
3. Guo, H.; Wang, F.; Zhang, L.; Luo, J. Technologies of energy router-based smart distributed energy network. *Proc. CSEE* **2016**, *36*, 3314–3324.
4. Liu, Y.; Yuan, D.; Gong, Z.; Jin, T.; Mohamed, M.A. Adaptive spectral trend based optimized EWT for monitoring the parameters of multiple power quality disturbances. *Int. J. Electr. Power Energy Syst.* **2023**, *146*, 108797. [[CrossRef](#)]
5. Zhao, D.; Hu, N.; Fu, J.; Ben, J.S.; Zi, N.Z. Research on the practice and road map of enhancing the flexibility of a new generation power system in China. *Power Syst. Prot. Control* **2020**, *53*, 1–9.
6. Loh, P.C.; Li, D.; Chai, Y.K.; Blaabjerg, F. Autonomous operation of hybrid microgrid with AC and DC subgrids. *IEEE Trans. Power Electron.* **2012**, *28*, 2214–2223. [[CrossRef](#)]
7. Zheng, L.; Chunming, T.; Fan, X.; Jun, G.; Songhui, X. The power control of power electronic transformer in hybrid AC-DC microgrid. *Trans. China Electrotech. Soc.* **2015**, *30*, 50–57.
8. Wang, S.; Su, S.; Wang, H.; Ouyang, Z.; Wang, H.; Zhou, W. An energy routing control method for a terminal energy router based on switching system theory. *Power Syst. Prot. Control* **2022**, *50*, 81–90.
9. Chen, R.; Yang, Y.; Jin, T. A hierarchical coordinated control strategy based on multi-port energy router of urban rail transit. *Prot. Control Mod. Power Syst.* **2022**, *7*, 15. [[CrossRef](#)]
10. Cui, X.; Jin, T.; Dai, Q. Research on Key Technologies of Energy Router for Urban Rail Transit. In Proceedings of the 2022 IEEE 5th International Conference on Electronics Technology (ICET), Chengdu, China, 16 May 2022; pp. 1250–1254.

11. Bu, Z.; Sun, X.; Teng, J.; Zhao, W.; Li, X.; Wang, B. A Compact Energy Router Scheme Based on MMC. *Proc. CSEE* **2022**, *42*, 4536–4546.
12. Li, P.; Sheng, W.; Duan, Q.; Li, Z.; Zhu, C.; Zhang, X. A Lyapunov Optimization-Based Energy Management Strategy for Energy Hub with Energy Router. *IEEE Trans. Smart Grid* **2020**, *11*, 4860–4870. [[CrossRef](#)]
13. Tu, C.; Lan, Z.; Luan, S.; Xiao, F. A Coordinated Power Control Strategy of Three-port DC Energy Router Based on Droop Phase-shift. *Power Syst. Technol.* **2019**, *43*, 4105–4114.
14. Hussain, S.M.S.; Aftab, M.A.; Nadeem, F.; Ali, I.; Ustun, T.S. Optimal Energy Routing in Microgrids with IEC 61850 Based Energy Routers. *IEEE Trans. Ind. Electron.* **2019**, *67*, 5161–5169. [[CrossRef](#)]
15. Cao, Y.; Yuan, L.; Zhu, S.; Huang, R.; Feng, G.; Zhao, Z. Parameter Design of Energy Router Orienting Energy Internet. *Power Syst. Technol.* **2015**, 3094–3101. [[CrossRef](#)]
16. Li, Z.; Sheng, W.; Duan, Q. Coordinated control strategy of AC/DC hybrid power router based on energy storage and voltage stabilization. *Autom. Electr. Power Syst.* **2019**, 121–129. [[CrossRef](#)]
17. Shi, L.; Liu, G. Research on switching control strategy for the multi-LAN-port energy router. *J. Electr. Power Sci. Technol.* **2015**, 3094–3101. [[CrossRef](#)]
18. Xu, M.; Tai, N.; Huang, W. Energy router design based on community energy network. *Power Syst. Prot. Control* **2016**, *44*, 177–183.
19. Li, S.; Wu, C.; Jiang, X.; Pan, P.; Ke, Z. Coordinated Control of Multiple Operation Conditions for Multi-port Energy Router in Energy Internet Framework. *Autom. Electr. Power Syst.* **2020**, *44*, 32–45.
20. Tu, C.; Xiao, F.; Lan, Z.; Guo, Q.; Shuai, Z. Analysis and Control of a Novel Modular-Based Energy Router for DC Microgrid Cluster. *IEEE J. Emerg. Sel. Top. Power Electron.* **2018**, *7*, 331–342. [[CrossRef](#)]
21. Xiao, Q.; He, J.; Wang, H.; Jia, H. Voltage balance control strategy for DC capacitor of electrical energy router under power grid failure. *Autom. Electr. Power Syst.* **2018**, *42*, 20–25.
22. Mansouri, S.A.; Nematbakhsh, E.; Ahmarinejad, A.; Jordehi, A.R.; Javadi, M.S.; Marzband, M. A hierarchical scheduling framework for resilience enhancement of decentralized renewable-based microgrids considering proactive actions and mobile units. *Renew. Sustain. Energy Rev.* **2022**, *168*, 112854. [[CrossRef](#)]
23. Nasir, M.; Jordehi, A.R.; Tostado-Véliz, M.; Tabar, V.S.; Mansouri, S.A.; Jurado, F. Operation of energy hubs with storage systems, solar, wind and biomass units connected to demand response aggregators. *Sustain. Cities Soc.* **2022**, *83*, 103974. [[CrossRef](#)]
24. Matin, S.A.A.; Mansouri, S.A.; Bayat, M.; Jordehi, A.R.; Radmehr, P. A multi-objective bi-level optimization framework for dynamic maintenance planning of active distribution networks in the presence of energy storage systems. *J. Energy Storage* **2022**, *52*, 104762. [[CrossRef](#)]
25. Zhang, Y.; Du, G.; Lei, Y.; Zheng, H. Current status and prospects of control strategy for a DC micro grid hybrid energy storage system. *Power Syst. Prot. Control.* **2021**, *49*, 177–187.
26. Ramos, F.; Pinheiro, A.; Nascimento, R.; de Araujo Silva, W., Jr.; Mohamed, M.A.; Annuk, A.; Marinho, M.H.N. Development of Operation Strategy for Battery Energy Storage System into Hybrid AC Microgrids. *Sustainability* **2022**, *14*, 13765. [[CrossRef](#)]
27. Nascimento, R.; Ramos, F.; Pinheiro, A.; Junior, W.d.A.S.; Arcanjo, A.M.C.; Filho, R.F.D.; Mohamed, M.A.; Marinho, M.H.N. Case Study of Backup Application with Energy Storage in Microgrids. *Energies* **2022**, *15*, 9514. [[CrossRef](#)]
28. Chen, W.; Liu, B.; Nazir, M.S.; Abdalla, A.N.; Mohamed, M.A.; Ding, Z.; Bhutta, M.S.; Gul, M. An Energy Storage Assessment: Using Frequency Modulation Approach to Capture Optimal Coordination. *Sustainability* **2022**, *14*, 8510. [[CrossRef](#)]
29. Dehghani, M.; Shiraz University of Technology; Montazeri, Z.; Givi, H.; Guerrero, J.; Dhiman, G.; University of Shahreza; Aalborg University; Government Bikram College of Commerce. Darts Game Optimizer: A New Optimization Technique Based on Darts Game. *Int. J. Intell. Eng. Syst.* **2020**, *13*, 286–294. [[CrossRef](#)]
30. Dehghani, M.; Montazeri, Z.; Dhiman, G.; Malik, O.; Morales-Menendez, R.; Ramirez-Mendoza, R.; Dehghani, A.; Guerrero, J.; Parra-Arroyo, L. A Spring Search Algorithm Applied to Engineering Optimization Problems. *Appl. Sci.* **2020**, *10*, 6173. [[CrossRef](#)]
31. Dhiman, G.; Oliva, D.; Kaur, A.; Singh, K.K.; Vimal, S.; Sharma, A.; Cengiz, K. BEPO: A novel binary emperor penguin optimizer for automatic feature selection. *Knowl. Based Syst.* **2020**, *211*, 106560. [[CrossRef](#)]
32. Dhiman, G. ESA: A hybrid bio-inspired metaheuristic optimization approach for engineering problems. *Eng. Comput.* **2019**, *37*, 323–353. [[CrossRef](#)]
33. Ali, A.I.M.; Alaas, Z.M.; Sayed, M.A.; Almalaq, A.; Farah, A.; Mohamed, M.A. An Efficient MPPT Technique-Based Single-Stage Incremental Conductance for Integrated PV Systems Considering Flyback Central-Type PV Inverter. *Sustainability* **2022**, *14*, 12105. [[CrossRef](#)]
34. Rao, C.; Hajjiah, A.; El-Meligy, M.A.; Sharaf, M.; Soliman, A.T.; Mohamed, M.A. A Novel High-Gain Soft-Switching DC-DC Converter with Improved P&O MPPT for Photovoltaic Applications. *IEEE Access* **2021**, *9*, 58790–58806. [[CrossRef](#)]
35. Mohamed, M.A.; Awwad, E.M.; El-Sherbeeney, A.M.; Nasr, E.A.; Ali, Z.M. Optimal scheduling of reconfigurable grids considering dynamic line rating constraint. *IET Gener. Transm. Distrib.* **2020**, *14*, 1862–1871. [[CrossRef](#)]

Disclaimer/Publisher’s Note: The statements, opinions and data contained in all publications are solely those of the individual author(s) and contributor(s) and not of MDPI and/or the editor(s). MDPI and/or the editor(s) disclaim responsibility for any injury to people or property resulting from any ideas, methods, instructions or products referred to in the content.